



CHORUS

This is the accepted manuscript made available via CHORUS. The article has been published as:

Heat Conduction Theory Including Phonon Coherence

Zhongwei Zhang, Yangyu Guo, Marc Bescond, Jie Chen, Masahiro Nomura, and Sebastian Volz

Phys. Rev. Lett. **128**, 015901 — Published 3 January 2022

DOI: [10.1103/PhysRevLett.128.015901](https://doi.org/10.1103/PhysRevLett.128.015901)

Heat conduction theory including phonon coherence

Zhongwei Zhang,^{1,*} Yangyu Guo,¹ Marc Bescond,² Jie Chen,^{3,†} Masahiro Nomura,¹ and Sebastian Volz^{1,2,3,‡}

¹*Institute of Industrial Science, The University of Tokyo, Tokyo 153-8505, Japan*

²*Laboratory for Integrated Micro and Mechatronic Systems,*

CNRS-IIS UMI 2820, The University of Tokyo, Tokyo 153-8505, Japan

³*Center for Phononics and Thermal Energy Science,*

School of Physics Science and Engineering and China-EU Joint Lab for Nanophononics,

Tongji University, Shanghai 200092, People's Republic of China

(Dated: December 7, 2021)

Understanding and quantifying the fundamental physical property of coherence of thermal excitations is a long-standing and general problem in physics. The conventional theory, i.e. the phonon gas model, fails to describe coherence and its impact on thermal transport. In this letter, we propose a general heat conduction formalism supported by theoretical arguments and direct atomic simulations, which takes into account both the conventional phonon gas model and the wave nature of thermal phonons. By naturally introducing wavepackets in the heat flux from fundamental concepts, we derive an original thermal conductivity expression including coherence times and lifetimes. Our theory and simulations reveal two distinct types of coherence, i.e., intrinsic and mutual, appearing in two different temperature ranges. This contribution establishes a fundamental frame for understanding and quantifying the coherence of thermal phonons, which should have a general impact on the estimation of the thermal properties of solids.

Phonons, i.e., quanta of vibrational waves, are commonly considered as one of the fundamental quasi-particles, simultaneously exhibiting wavelike and particlelike characteristics in nanostructured crystals or bulk materials. The wavelike behavior of phonons impacts thermal properties via coherence mechanisms, as highlighted by several pioneering [1, 2] and recent works [3, 4]. The particlelike behavior has been treated by Boltzmann transport equation (BTE) and the phonon-gas model in most solids [5–10]. Experiments [1, 2, 11–13] have revealed, however, that the wave nature of thermal phonons plays a substantial role in thermal transport, as for example, in the observations of coherent thermal transport in nano-phononic crystals [1, 2, 11, 12]. Later, theoretical and simulation studies [14–18] were devoted to the understanding of phonon coherence, such as the one producing band folding [19–21], but missing the particle behavior. Recently, the theoretical study [22] revealed that the realistic phonon dynamics can only be manifested if both intrinsic coherence relevant to the extension of phonon wavepackets and the particlelike behavior of thermal phonons are taken into account.

The conventional BTE also fails in complex crystals, as a pure particle picture cannot yield a complete description of thermal conductivity, such as in Ti_3VSe_4 [23, 24]. Recently, Simoncelli *et al.* [3] developed a theory for thermal transport in glasses and complex crystals, in which the coherence between densely packed phonon branches contributes to thermal transport. A similar approach has been developed by Isaeva *et al.* [4] as well at the same time. This mutual coherence among branches is identi-

fied as an additional phonon wave-relevant term [25–27]. The picture of this mutual coherence, that might be compared to a hopping process, however remains physically unclear. Finally, quantifying the full coherence of thermal phonons and its effect on heat conduction remains a critical issue in transport physics.

In this letter, a general heat conduction theory is proposed to establish an original expression for the thermal conductivity that includes the full coherent nature of phonon excitations. This expression involves both phonon lifetimes and coherence times. Those are obtained by tracking the real phonon dynamics and using a wavelet transform of the atomic trajectories during an equilibrium molecular dynamic (EMD) simulation. We show that the predictions of our theory yield significant differences from those of the conventional phonon-gas model, as demonstrated in the Ti_3VSe_4 case (See atomic structure in Fig. 1(a)). We find that there are two types of coherence, i.e., intrinsic and mutual, which take a critical role over different temperature regions. These conclusions open unexpected insights on the reality of thermally activated phonon modes and the importance of the diverse coherence mechanisms when assessing thermal properties.

The thermal conductivity (κ) can be calculated based on the Green-Kubo approach with the autocorrelation of the heat flux $\mathbf{S}(t)$ as [28]

$$\kappa = \frac{V}{3k_B T^2} \int \langle \mathbf{S}(t) \cdot \mathbf{S}(0) \rangle dt, \quad (1)$$

where V corresponds to the system volume, k_B is the Boltzmann constant and T the temperature. We now define the heat flux component \mathbf{S}_λ corresponding to the contribution of mode λ to the total heat flux, i.e., $\mathbf{S}(t) = \sum_\lambda \mathbf{S}_\lambda(t)$. λ refers to a specific mode of wavevector \mathbf{k} and

* zhongwei@iis.u-tokyo.ac.jp

† jie@tongji.edu.cn

‡ volz@iis.u-tokyo.ac.jp

of the branch s , which implies that the correlation can operate between modes of different wavevectors and of different branches. Then, the thermal conductivity can be decomposed as follows

$$\kappa_d = \frac{V}{3k_B T^2} \sum_{\lambda} \int \langle \mathbf{S}_{\lambda}(t) \cdot \mathbf{S}_{\lambda}(0) \rangle dt. \quad (2)$$

As discussed before by Gill-Comeau and Lewis [29, 30], the neglected off-diagonal part corresponds to the collective excitations of phonons ($\sim \langle \mathbf{S}_{\lambda}(t) \cdot \mathbf{S}_{\lambda' \neq \lambda}(0) \rangle$). In most solids, κ_d defined in Eq. (2) is predominant and the off-diagonal terms only become significant in the hydrodynamic regime [9, 31–33], for instance in graphene and graphite. Therefore, the diagonal thermal conductivity only will be addressed in the following. Based on the definition of the harmonic heat flux operator [34], $\mathbf{S} = \frac{1}{V} \sum_{\lambda} N_{\lambda} \hbar \omega_{\lambda} \mathbf{v}_{\lambda}$, the thermal conductivity can be derived as

$$\kappa = \frac{1}{3k_B V T^2} \sum_{\alpha} \sum_{\lambda} \hbar^2 \omega_{\lambda}^2 v_{\lambda, \alpha}^2 N_{\lambda}^2 \int Cor_{\lambda}(t) dt, \quad (3)$$

here, \hbar denotes the reduced Planck constant, ω_{λ} is the eigenfrequency, \mathbf{v}_{λ} the group velocity of mode λ and α the Cartesian coordinate. $N_{\lambda}(t)$ is the time-dependent phonon number of mode λ and $Cor_{\lambda}(t) = \frac{\langle N_{\lambda}(t) N_{\lambda}(0) \rangle}{\langle N_{\lambda}(0) N_{\lambda}(0) \rangle}$ the phonon decay. Considering the classical definition of the phonon number $N_{\lambda} = \frac{k_B T}{\hbar \omega_{\lambda}}$, Eq. (3) reduces to $\kappa = \frac{1}{3} \sum_{\alpha} \sum_{\lambda} C_{v, \lambda}^{clas} v_{\lambda, \alpha}^2 \int Cor_{\lambda}(t) dt$, where $C_{v, \lambda}^{clas} = \frac{k_B}{V}$ is the classical specific heat per mode. When the particle-like behavior predominates, $Cor_{\lambda}(t)$ follows an exponential decay law with the lifetime τ_{λ}^p according to the conventional single-mode relaxation time (SMRT) approximation [8, 10], that is $Cor_{\lambda}(t) = e^{-\frac{t}{\tau_{\lambda}^p}}$. After integration, the classical particlelike thermal conductivity can be expressed as follows

$$\kappa_p = \frac{1}{3} \sum_{\alpha} \sum_{\lambda} C_{v, \lambda}^{clas} v_{\lambda, \alpha}^2 \tau_{\lambda}^p. \quad (4)$$

Equation (4) is analogous to the commonly used Peierls-Boltzmann formula [6]. However, as the coherence effect increases, a correction should be considered in the description of the phonon decay by including the modal coherence time (τ_{λ}^c) [22] as follows

$$Cor_{\lambda}(t) = e^{-\frac{t}{2\tau_{\lambda}^p}} e^{-4 \ln 2 \frac{t^2}{\tau_{\lambda}^c e^2}}. \quad (5)$$

The second gaussian term originates from the interference between different modes, expressing coherence effects in the phonon dynamics. Consequently, by integrating Eq. (5), the complete thermal conductivity (κ_{p+w}) including the wavelike behavior can be expressed as

$$\kappa_{p+w} = \frac{1}{3} \sum_{\alpha} \sum_{\lambda} C_{v, \lambda}^{clas} v_{\lambda, \alpha}^2 \sqrt{\frac{\pi}{4 \ln 2}} \tau_{\lambda}^c e^{\frac{\tau_{\lambda}^c{}^2}{128 \ln 2 \tau_{\lambda}^p{}^2}}. \quad (6)$$

When setting $\tau_{\lambda}^p = \tau_{\lambda}^c$, Eq. (6) reduces to the conventional Peierls-Boltzmann formula with a corrective coefficient ≈ 1.07 . This consideration reveals that equality between coherence time and lifetime [35] is underlying the traditional phonon gas model.

In realistic systems, the scatterings are diverse and can also be incorporated into the model of Matthiessen

$$\frac{1}{\tau_{\lambda}^{total}} = \frac{1}{\tau_{\lambda}^{ph-ph}} + \frac{1}{\tau_{\lambda}^{isotope}} + \frac{1}{\tau_{\lambda}^{boundary}}. \quad (7)$$

where, τ_{λ}^{ph-ph} refers to the phonon decay time for τ_{λ}^p and $\sqrt{\frac{\pi}{4 \ln 2}} \tau_{\lambda}^p e^{\frac{\tau_{\lambda}^c{}^2}{128 \ln 2 \tau_{\lambda}^p{}^2}}$ in Eq. (4) and Eq. (6), respectively. The calculations of the isotope scattering time $\tau_{\lambda}^{isotope}$ [36] and of the boundary scattering time $\tau_{\lambda}^{boundary}$ [37] follow the reference [38]. Only the isotope scattering is intrinsically considered in our following calculations. Quantifying the contribution of coherence as proposed in Eq. (6) requires the knowledge of lifetimes and coherence times. These quantities are accessible by a wavelet approach [22, 39, 40].

The developed model is then applied to the complex crystal Ti_3VSe_4 (See atomic structure in Fig. 1(a)). In order to collect accurate phonon information from MD simulations, a machine learning potential (MLP) [41, 42] is adopted after being trained by *ab initio* MD simulations [43–47]. In the Supplementary Materials (SM) [39], the training process and the verification of the MLP are described [38, 48–50]. All MD simulations using the MLP are performed with the LAMMPS package [51], which is mainly used for calculating MD thermal conductivity [28, 52] for comparison (See Sec. S2.3 in [39]), and for extracting the atomic information for subsequent wavelet transform calculations (See Sec. S3 in [39] for details).

By applying the wavelet transform approach, we can firstly obtain the evolution time and coherence time dependent phonon number $N(t_0, \tau_{\lambda}^c)$. Increase temperature usually dephases the correlation of phonon waves or suppresses the coherent/wavelike behaviour, resulting in a decrease in coherence time. The coherence time of the 0.25 THz mode in Ti_3VSe_4 , for example, decreases when the temperature rises from 100 K to 300 K (See Fig. S5). This dephasing trend has already been seen in bulk graphene [22] and superlattices [1, 17, 53] before which corresponds to a loss of ‘intrinsic’ coherence. **The intrinsic coherence refers to the spatial or temporal extension of each phonon wave-packet, which results from the interference between plane waves [22] and explained the coherent thermal transport in superlattices [54].** However, for high frequency phonons in Ti_3VSe_4 , e.g., at 0.93 THz shown in Fig. 1(c), the coherence time

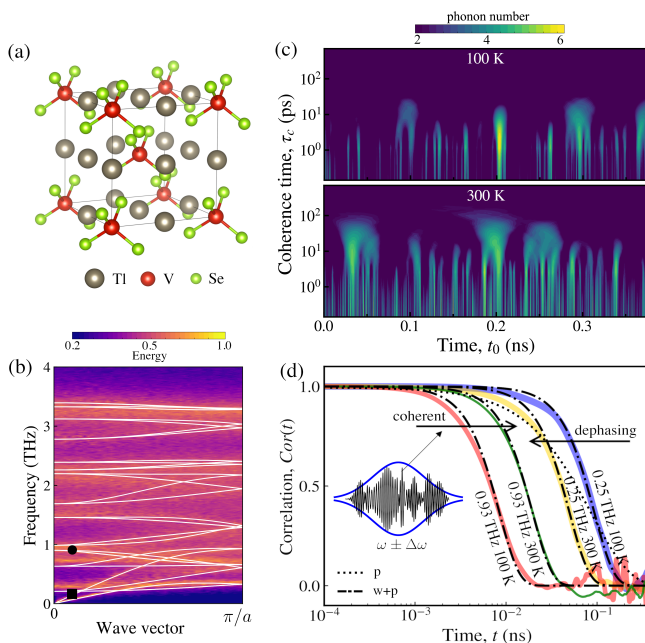


FIG. 1. (a) The conventional lattice of Tl_3VSe_4 . (b) The phonon dispersion of Tl_3VSe_4 from lattice dynamic calculations (white lines) and room-temperature spectral energy density calculations (contour) for the conventional cell along $\Gamma(0, 0, 0) \rightarrow M(0.5, 0, 0)$. a denotes the lattice constant. The symbols in (b) indicate the modes being analyzed, 0.25 THz (square) and 0.93 THz (circle). (c) Evolution time and coherence time dependent phonon number (contour) of Tl_3VSe_4 for the 0.93 THz mode at 100 K and 300 K. (d) Phonon decay (correlation) versus correlation time in Tl_3VSe_4 for the 0.25 and 0.93 THz modes at 100 K and 300 K. The dash-dotted lines (p+w) show the fitting by Eq. (5). The dotted line (p) shows the fitting by the conventional exponential decay. The inset of (d) shows the realistic wavepacket of the mode 0.93 THz resulting from the combination of shorter wavepackets at 300 K.

reversely increases with temperature, as evidenced by the expanded ‘clouds’ and their shift into a higher coherence time regime. These ‘clouds’ can be understood as the coherence effect between the modes of different branches in the phonon dispersion (Fig. 1(b)), as demonstrated before by Simoncelli *et al.* [3] and Isaeva *et al.* [4]. The clouds with long coherence times are connected to the packets with small coherence times, as if the former were generated by the latter.

The abundance of small wavepackets with shorter lifetimes is partially originating from the temperature induced phonon-phonon scattering. Since lifetime is reversely proportional to the frequency broadening (i.e. $\Delta\omega$), the enlarged linewidth of the dispersion curves associated with reduced frequency intervals between branches promote smaller wavepackets as illustrated by Figs. 1(b-c). In a subsequent stage, due to their large number, those small wavepackets have higher probability to establish a phase relation between themselves, which results in the generation of wavepackets with large coher-

ence times, referred to as ‘clouds’ above (See the inset of Fig. 1(d)). This argument does not only support the model of Simoncelli *et al.* [3], but also offers a physical picture of the mutual coherence for phonons in complex crystals. In addition, this effect should also be amplified as temperature further rises due to the increase of branches broadening from phonon-phonon scatterings. The temperature effects in Figs. 1(c-d) and Fig. S5 indicate that the increase of mutual coherence for the high frequency mode crucially depends on an enhanced branch density, as smaller wavepackets with the same wavevector but a lower frequency also appear but do not exhibit an increased coherence. Note that these tendencies are also respectively observed in other low or high frequency modes.

Coherence is expected to have critical impact on the phonon decay and its propagation. The phonon decay can be extracted from the autocorrelation function of the phonon number $N(t_0, \tau_\lambda^c)$, as displayed in Fig. 1(d). The details of the computations are provided in [39]. When including the coherence effect, the phonon decay should follow the generalized law of Eq. (5) as we demonstrated before [22]. From the fitted particle-related decay (dotted line) to the coherence corrected decay (dash-dotted line) of Fig. 1(d), the coherence appears as a delay to the conventional exponential decay due to the temporal extension of phonon wavepackets [22]. Both their intrinsic coherence and the one resulting from the phase correlation between several wavepackets, namely mutual coherence, yield a delay in phonon decay. In addition, the phonon decay of the low frequency 0.25 THz mode shows the temperature effects on the coherence dephasing and reduction of phonon lifetimes. In contrast, for the high frequency 0.93 THz at which branch density is high (See the density of states in Fig. S6), the increase of temperature contributes to coherence, producing a further delay in phonon decay. The inset of Fig. 1(d) shows how small wavepackets combine into a large one in this frequency range. By fitting this phonon decay with the generalized decay law of Eq. (5), we obtain τ_λ^p and τ_λ^c for different modes as reported in Fig. S6. The fitting details can be found in [39]. A \mathbf{q} -grid of $16 \times 16 \times 16$ is applied to analyze the modes in the full Brillouin zone, this mesh is yielding converged results in BTE based estimations. Importantly, τ_λ^c becomes larger than τ_λ^p in the region of relatively high frequencies, because of the coherence effect (See Fig. S6).

Due to the predominance of phonons of low frequencies, the effect of quantum population on the transport properties of Tl_3VSe_4 is limited. The thermal conductivities of Eqs. (4) and (6) are expressed with the classical population (i.e. $\kappa_{p/p+w}^{clas}$), which can be quantum corrected (i.e. $\kappa_{p/p+w}^{qua}$) by replacing $C_{v,\lambda}^{clas}$ with the quantum specific heat $C_{v,\lambda}^{qua}$, here $C_{v,\lambda}^{qua} = \frac{k_B \exp(x)}{V} \left[\frac{x}{\exp(x)-1} \right]^2$ with $x = \frac{\hbar\omega_\lambda}{k_B T}$. At low temperatures, Fig. 2(a) reports that the delay effect on phonon decay due to the intrinsic coherence leads to substantial contributions to thermal

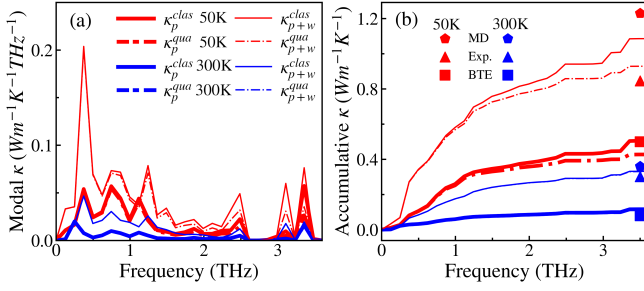


FIG. 2. Modal thermal conductivity of Tl_3VSe_4 . (a) Modal classical and quantum thermal conductivities of Tl_3VSe_4 at 50 K and 300 K. (b) Accumulative classical and quantum thermal conductivities of Tl_3VSe_4 at 50 K and 300 K. The symbols refer to experimental results (Exp.) [23], Boltzmann transport equation results (BTE) [26] and our molecular dynamic simulations (MD).

conductivity in the full frequency range. The effect of intrinsic coherence should be weakened by increasing temperature. The wavelike contributions are still prominent at 300 K and the additional components are migrating to the region after 0.25 THz where the dense branches and mutual coherence emerge. Obviously, coherence can correct thermal conductivities by incorporating the wavelike contribution, and coherence behaviors are different at low temperatures (intrinsic coherence) and at high temperatures (mutual coherence).

The accumulative κ in Fig. 2(b) further evidences the importance of wavelike contributions to thermal conductivities in Tl_3VSe_4 . Here, the BTE results are from Jain [26], in which a temperature dependent effective potential (TDEP) is considered. As all scatterings and temperature effects are included in MD simulations, our predicted $\kappa_p^{clas/qua}$ (thicker lines) are in reasonable agreement with the BTE results (square symbols), indicating the validity of the particle description in our model. When including the wavelike behaviour of thermal phonons, the corrected $\kappa_{p+w}^{clas/qua}$ approximate to both the experimental measurements [23] and the direct MD simulations, especially at 300 K. The limited discrepancies at 50 K are mostly originating from the classical population of phonons in MD simulation, which overestimates phonon-phonon scatterings while underestimating κ_p^{clas} and κ_{p+w}^{clas} with suppressed τ_λ^p and τ_λ^c .

For overall comparison, thermal conductivities based on our direct MD simulations, experimentally measured values [23] and the BTE calculations with TDEP [26] are summarized in Fig. 3(a). MD simulations implicitly include all orders of anharmonicity for phonon-phonon scattering as well as both the wavelike and particle-like behaviors of phonons. Consequently, EMD simulations include the real phonon dynamics and well coincide with the experimental κ , indicating the accuracy of our MLP. The computed particlelike thermal conductivities ($\kappa_p^{clas/qua}$) agree well with the BTE results, but remains lower than the experimental measurements, indi-

ating the failure of BTE in capturing phonon coherence of Tl_3VSe_4 . As we further include the wavelike contribution by applying the revised heat conduction law of Eq. (6), the thermal conductivities significantly increase. The wavelike corrected values $\kappa_{p+w}^{clas/qua}$ agree well with the experimental measurements and MD simulations in the full temperature region. This comparison indicates that the proposed model is sufficient in predicting thermal transport by including the wavelike features of phonons.

The degree of coherence correction to thermal conductivity is further estimated in Fig. 3(b) as $\frac{\kappa_{p+w}^{clas/qua} - \kappa_p^{clas/qua}}{\kappa_{p+w}^{clas/qua}} \times 100\%$. Interestingly, a non-monotonic dependence of the coherence contribution as a function of temperature is observed, which agrees well with the above demonstration of the coexistence of two types of coherence. At room-temperature, the wavelike correction reaches 66 %. The trend of the correction with temperature coincides with the discrepancy between the prevailing BTE theory and the real phonon dynamics observed in the experiments and MD simulations of Fig. 3(a), revealing that the wavelike behavior becomes more significant at low and high temperatures. Jain [26] found that the conductivities including coherence as proposed by Simoncelli *et al.* [3], remain close to the experimental measurements when considering uncertainties. The discrepancy still appears at low temperatures where intrinsic coherence becomes important (See the comparison in [39]). The used Allen and Feldman (AF) model [55, 56] and Cahill-Watson-Pohl (CWP) model [57, 58], as well as the theory from [3], are based on the weakly propagating modes and the inter-modes ‘hopping’ additionally contributing to thermal transport in complex crystals or disordered systems. The discovered mutual coherence offers direct evidence on how modes interact and

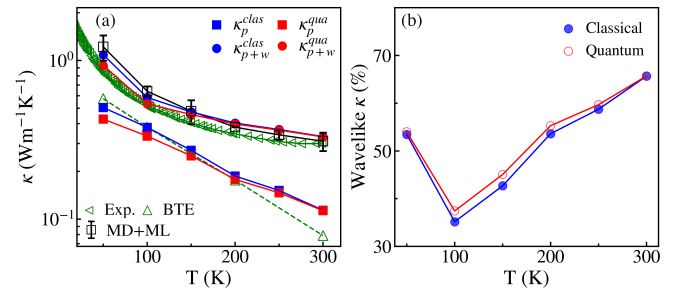


FIG. 3. Comparison of thermal conductivities of Tl_3VSe_4 from different approaches. (a) The comparison of thermal conductivities of Tl_3VSe_4 versus temperature. The left oriented triangles are experimental results (Exp.) [23], the upward triangles refer to BTE results [26] and the squares correspond to our machine learning based MD simulations (MD+ML). Full symbols denote the models of Eq. (4) (squares) and of our theory of Eq. (6) (circles) in the classical (blue) and the quantum (red) approximations. (b) The additional contribution of coherence to thermal conductivities of Tl_3VSe_4 versus temperature.

affect the thermal transport. The above comparisons between thermal conductivities demonstrate the remaining issues of prevailing theories and indicate the ability of our model to capture both wavelike and particlelike pictures of phonons in thermal transport. The agreement with measurements especially provides a satisfactory test of our theory based on experimental data. **The collective thermal conductivity (i.e., off-diagonal terms in Eq. (1)) is also studied in Sec. S6 of the SM [39]. The low contribution of collective excitations, even at 50 K, indicates the predominance of Umklapp phonon-phonon scattering in this complex crystal.**

Coming back to the fundamental definition of the heat flux, we have established a new expression of the thermal conductivity including phonon coherence via coherence time. The estimation of this generalized thermal conductivity was implemented by introducing a wavelet transformation of MD quantities, which offers the coherence time of phonon excitations as well as their lifetimes. This methodological treatment of coherence in heat conduction has hence unraveled the rich content of coherent effects on thermal transport. This previously uncharted information has led to quantitative estimation of the impact of coherence responsible for a 66 % increase of ther-

mal conductivity at room-temperature for complex crystal Tl_3VSe_4 . In addition, two distinct types of coherence are observed in our explorations, including intrinsic coherence and mutual coherence, which can be simultaneously modeled by our heat conduction theory. **We also believe that our theory opens to a broad range of applications in other complex crystals, simple crystals (See Sec. S7 in [39]) and amorphous materials (See preprint in [59]).** In short, we proposed a novel paradigm to describe the full coherence of phonon heat carriers, which has a global repercussion in the assessment of the thermal properties in nanostructures as well as in bulk materials.

ACKNOWLEDGMENTS

This work is partially supported by CREST JST (No. JPMJCR19I1 and JPMJCR19Q3). This research used the computational resources of the Oakforest-PACS supercomputer system, The University of Tokyo. This project is also supported in part by the grants from the National Natural Science Foundation of China (Grant Nos. 12075168 and 11890703), and Science and Technology Commission of Shanghai Municipality (Grant No. 19ZR1478600).

-
- [1] M. N. Luckyanova, J. Garg, K. Esfarjani, A. Jandl, M. T. Bulsara, A. J. Schmidt, A. J. Minnich, S. Chen, M. S. Dresselhaus, and Z. Ren, *Science* **338**, 936 (2012).
 - [2] J. Ravichandran, A. K. Yadav, R. Cheaito, P. B. Rossen, A. Soukiassian, S. J. Suresha, J. C. Duda, B. M. Foley, C. H. Lee, Y. Zhu, A. W. Lichtenberger, J. E. Moore, D. A. Muller, D. G. Schlom, P. E. Hopkins, A. Majumdar, R. Ramesh, and M. A. Zurbuchen, *Nat. Mater.* **13**, 168 (2014).
 - [3] M. Simoncelli, N. Marzari, and F. Mauri, *Nat. Phys.* **15**, 809 (2019).
 - [4] L. Isaeva, G. Barbalinardo, D. Donadio, and S. Baroni, *Nat. Commun.* **10**, 3853 (2019).
 - [5] R. Peierls, *Ann. Phys.* **395**, 1055 (1929).
 - [6] J. M. Ziman, *Electrons and phonons: the theory of transport phenomena in solids* (Oxford university press, 2001).
 - [7] R. A. Guyer and J. A. Krumhansl, *Phys. Rev.* **148**, 766 (1966).
 - [8] A. J. McGaughey and M. Kaviani, *Phys. Rev. B* **69**, 943031 (2004).
 - [9] A. Cepellotti and N. Marzari, *Phys. Rev. X* **6**, 041013 (2016).
 - [10] A. J. Minnich, *J. Condens. Matter Phys.* **27**, 053202 (2015).
 - [11] N. Zen, T. A. Puurtinen, T. J. Isotalo, S. Chaudhuri, and I. J. Maasilta, *Nat. Commun.* **5**, 3435 (2014).
 - [12] J. Maire, R. Anufriev, R. Yanagisawa, A. Ramiere, S. Volz, and M. Nomura, *Sci. Adv.* **3**, e1700027 (2017).
 - [13] R. Hu, S. Iwamoto, L. Feng, S. Ju, S. Hu, M. Ohnishi, N. Nagai, K. Hirakawa, and J. Shiomi, *Phys. Rev. X* **10**, 21050 (2020).
 - [14] Z. Tian, K. Esfarjani, and G. Chen, *Phys. Rev. B* **89**, 235307 (2014).
 - [15] Y. Wang, H. Huang, and X. Ruan, *Phys. Rev. B* **90**, 48 (2014).
 - [16] J. Mendoza and G. Chen, *Nano Lett.* **16**, 7616 (2016).
 - [17] S. Hu, Z. Zhang, P. Jiang, J. Chen, S. Volz, M. Nomura, and B. Li, *J. Phys. Chem. Lett.* **9**, 3959 (2018), 1602.05057.
 - [18] T. Juntunen, O. Vänskä, and I. Tittonen, *Physical Review Letters* **122**, 105901 (2019).
 - [19] H. Maris and Y. Tanaka, *Phys. Rev. B* **60**, 2627 (1999).
 - [20] W. E. Bies, R. J. Radtke, and H. Ehrenreich, *J. Appl. Phys.* **88**, 1498 (2000).
 - [21] M. Maldovan, *Nat. Mater.* **14**, 667 (2015).
 - [22] Z. Zhang, Y. Guo, M. Bescond, J. Chen, M. Nomura, and S. Volz, *Phys. Rev. B* **103**, 184307 (2021).
 - [23] S. Mukhopadhyay, D. S. Parker, B. C. Sales, A. A. Puretzky, M. A. McGuire, and L. Lindsay, *Science* **360**, 1455 (2018).
 - [24] Y. Luo, X. Yang, T. Feng, J. Wang, and X. Ruan, *Nat. Commun.* **11**, 2554 (2020).
 - [25] Y. Xia, K. Pal, J. He, V. Ozoliņš, and C. Wolverton, *Phys. Rev. Lett.* **124**, 065901 (2020).
 - [26] A. Jain, *Phys. Rev. B* **102**, 201201(R) (2020).
 - [27] R. Hanus, J. George, M. Wood, A. Bonkowski, Y. Cheng, D. L. Abernathy, M. E. Manley, G. Hautier, G. J. Snyder, and R. P. Hermann, *Mater. Today Phys.* **18**, 100344 (2021).
 - [28] R. Kubo, *Rep. Prog. Phys.* **29**, 255 (1966).
 - [29] M. Gill-Comeau and L. J. Lewis, *Appl. Phys. Lett.* **106**, 193104 (2015).

- [30] M. Gill-Comeau and L. J. Lewis, *Phys. Rev. B* **92**, 195404 (2015).
- [31] Y. Guo and M. Wang, *Phys. Rep.* **595**, 1 (2015).
- [32] Z. Ding, J. Zhou, B. Song, V. Chiloyan, M. Li, T. H. Liu, and G. Chen, *Nano Lett.* **18**, 638 (2018).
- [33] Z. Zhang, Y. Ouyang, Y. Guo, T. Nakayama, M. Nomura, S. Volz, and J. Chen, *Phys. Rev. B* **102**, 195302 (2020).
- [34] R. J. Hardy, *Phys. Rev.* **132**, 168 (1963).
- [35] B. Latour and Y. Chalopin, *Phys. Rev. B* **95**, 214310 (2017).
- [36] S.-I. Tamura, *Phys. Rev. B* **27**, 858 (1983).
- [37] H. B. G. Casimir, *Physica* **5**, 495 (1938).
- [38] W. Li, J. Carrete, N. A. Katcho, and N. Mingo, *Comput. Phys. Commun.* **185**, 1747 (2014).
- [39] See Supplemental Material [url] for (1) Construction of MLP. (2) Benchmarks of MLP, including phonon dispersion, BTE calculations and MD simulations. (3) Wavelet transform. (4) Density of states. (5) Phonon decay formalism. (6) Thermal conductivity from collective terms. (7) Thermal conductivity of graphene. (8) Deviation between BTE and experimental data, which includes Refs. [60–65].
- [40] The code providing the thermal conductivity computed with coherence effects according to our model can be found as an open-source package in <https://github.com/ZhongweiZhangsite/WPPT>.
- [41] A. V. Shapeev, *Multiscale Model and Sim.* **14**, 1153 (2016).
- [42] I. S. Novikov, K. Gubaev, E. V. Podryabinkin, and A. V. Shapeev, *Mach. learn.: sci. technol.* **2**, 025002 (2021).
- [43] G. Kresse and J. Hafner, *Phys. Rev. B* **47**, 558 (1993).
- [44] G. Kresse and J. Furthmüller, *Phys. Rev. B* **54**, 11169 (1996).
- [45] G. Kresse and J. Furthmüller, *Comput. Mater. Sci.* **6**, 15 (1996).
- [46] G. Kresse and J. Hafner, *J. Condens. Matter Phys.* **6**, 8245 (1994).
- [47] A. Jain and A. J. McGaughey, *Comput. Mater. Sci.* **110**, 115 (2015).
- [48] W. Li, L. Lindsay, D. A. Broido, D. A. Stewart, and N. Mingo, *Phys. Rev. B* **86**, 174307 (2012).
- [49] A. Togo and I. Tanaka, *Scr. Mater.* **108**, 1 (2015).
- [50] Y. Ouyang, Z. Zhang, C. Yu, J. He, G. Yan, and J. Chen, *Chin. Phys. Lett.* **37**, 126301 (2020).
- [51] S. Plimpton, *J. Comput. Phys.* **117**, 1 (1995).
- [52] D. Torii, T. Nakano, and T. Ohara, *J. Chem. Phys.* **128**, 44504 (2008).
- [53] X. K. Chen, Z. X. Xie, W. X. Zhou, L. M. Tang, and K. Q. Chen, *Appl. Phys. Lett.* **109**, 107 (2016).
- [54] B. Latour, S. Volz, and Y. Chalopin, *Phys. Rev. B* **90**, 014307 (2014).
- [55] P. B. Allen and J. L. Feldman, *Phys. Rev. Lett.* **62**, 645 (1989).
- [56] P. B. Allen and J. L. Feldman, *Phys. Rev. B* **48**, 12581 (1993).
- [57] D. G. Cahill and R. O. Pohl, *Solid State Commun.* **70**, 927 (1989).
- [58] D. G. Cahill, S. K. Watson, and R. O. Pohl, *Phys. Rev. B* **46**, 6131 (1992).
- [59] Z. Zhang, Y. Guo, M. Bescond, J. Chen, M. Nomura, and S. Volz, Strong phase correlation between diffusons governs heat conduction in amorphous silicon (2021), arXiv:2110.10487.
- [60] J. M. Larkin, J. E. Turney, A. D. Massicotte, C. H. Amon, and A. J. McGaughey, *Journal of Computational and Theoretical Nanoscience* **11**, 249 (2014).
- [61] S. Chen, A. L. Moore, W. Cai, J. W. Suk, J. An, C. Mishra, C. Amos, C. W. Magnuson, J. Kang, L. Shi, and R. S. Ruoff, *ACS Nano* **5**, 321 (2011).
- [62] S. Chen, Q. Wu, C. Mishra, J. Kang, H. Zhang, K. Cho, W. Cai, A. A. Balandin, and R. S. Ruoff, *Nat. Mater.* **11**, 203 (2012).
- [63] X. Gu, Z. Fan, H. Bao, and C. Y. Zhao, *Phys. Rev. B* **100**, 064306 (2019).
- [64] L. Lindsay and D. A. Broido, *Phys. Rev. B* **81**, 205441 (2010).
- [65] Z. Fan, W. Chen, V. Vierimaa, and A. Harju, *Comput. Phys. Commun.* **218**, 10 (2017).